RSC Advances

ROYAL SOCIETY OF CHEMISTRY

www.rsc.org/advances

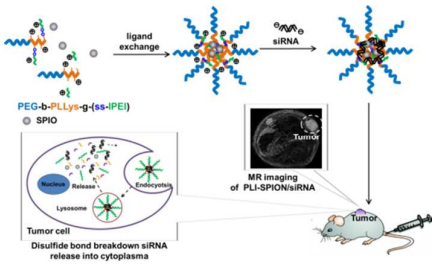

A biodegradable nanocarrier, PLI-SPION, was used to simultaneously deliver survivin-specific siRNA and MRI contrast agent SPIO.

Cite this: DOI: 10.1039/c0xx00000x

www.rsc.org/xxxxxx

ARTICLE TYPE

Effective siRNA therapy of hepatoma mediated by a nonviral vector with MRI-visibility and biodegradability

Jin Wang,[a] Linglan Ren, [a,b] Jingguo Li, [b] Jinsheng Huang, [b] Du Cheng, *[b] and Xintao Shuai *[b,c]

Received (in XXX, XXX) Xth XXXXXXXXX 20XX, Accepted Xth XXXXXXXXX 20XX

DOI: 10.1039/b000000x

Although RNA interference (RNAi) has demonstrated great potential in tumor therapy in recent years, the lack of effective approach for non-invasive monitoring of the in *vivo* siRNA delivery is still impeding its clinical application. Based on the biodegradable and redox-sensitive cationic polymer synthesized in our lab, an MRI-visible nanocarrier was prepared to codeliver siRNA and SPIO into HepG2 cancer cells. The highly efficient codelivery of siRNA and SPIO were achieved both in vitro and vivo. Consequently, the survivin-specifc siRNA delivered with the vector could effectively suppress the survivin gene expression and promote hepatic tumor cell apoptosis. Moreover, incorporation of SPIO made the siRNA delivery and therapy trackable with the noninvasive magnetic resonance imaging (MRI), which in turn may provide real-time and reliable information to guide the optimization of carrier properties for targeted siRNA delivery.

1. Introduction

Theranostics, a term employed to depict an emerging concept in disease treatment, has got more and more attention in recent years. [1] By integrating the diagnostic and therapeutic agents into one nanomedicinal system, theranostics provides a platform for conducting the diagnosis and therapy simultaneously, which makes the dosage design more accurate and reliable.[2] So far, different drugs including small interfering RNA (siRNA) and small molecular anticancer drugs (e.g. doxorubincin and paclitaxel) have been incorporated with MRI contrast agents such as superparamagnetic iron oxide (SPIO) to generate theranostics.[3-10]

On the other hand, RNA interference with siRNA has demonstrated positive therapeutic effect in various disease models including cancer and viral infection.[11-12] For instance, down-regulation of the survivin gene by survivin-specific siRNA induced the cancer cell apoptosis and death.[13-16] Although promising, the lack of effective siRNA delivery approaches still remains a bottleneck for the clinical applications of this therapeutic approach since siRNA is prone to biodegradation in bloodstream and is hard to cross the cell membrane.[17] To solve the problem, many cationic polymers like polyethylenimine (PEI) and poly(L-lysine) (PLL) have been applied to deliver the nucleic acids (siRNA and pDNA) into various types of cells.[18-19] In particular, the diblock copolymer of PEI and poly(ethylene glycol) (PEG-PEI), has demonstrated great potential as an effective carrier for tumor gene therapy and immunosuppression after organ transplantation.[9] In our recent work, siRNA targeting survivin gene was delivered into cancer cells by PEG-PEI polymer, which resulted in tumor growth suppression.[10] Considering that high molecular weight PEI generally used in nucleic acid delivery could not be degraded in vivo and thus may lead to accumulative toxicity after use, we further attempted to develop biodegradable carriers with better biosafety and meanwhile good delivery efficiency. Through reducible disulfide linkage, linear polyethylenimine (lPEI) with small molecular weight was grafted onto the copolymer of poly(ethylene glycol) and poly(L-lysine) to yield a ternary copolymer named PLI.[18] By this means, the biodegradability of PLL and proton buffering of PEI was combined into one delivery system. The disulfide linkage can be cleaved quickly inside the tumor cells with the 1000 fold high glutathione concentration compared to that in bloodstream.[20]

In addition to the difficulty in preparing effective vectors for siRNA delivery, evaluation of the in vivo siRNA delivery efficiency and biodistribution is a big challenge as well. Conventional methods such as ex vivo histopathology could not provide real-time information on drug delivery efficiency, distribution and therapeutic effect. In comparison, noninvasive imaging approaches such as MRI demonstrated great potential for real-time detection of carrier-mediated drug delivery.[1] MRI is currently playing an important role in early detection of hepatocellular carcinoma (HCC) as well as differentiation diagnosis among HCC, degeneration nodular hyperplasia and adenoma in clinical practices. A kind of liver sensitive MRI contrast agent, the superperamagnetic iron oxide (SPIO), could be detected at micromolar concentrations of iron to offer sufficient sensitivity for T_2-weighted imaging.[21-22] However, SPIO nanoparticles (SPIONs) are commonly coated by a hydrophobic layer of surfactant molecules, and thus the hydrophobic surface of SPIONs limited its application in vivo due to its poor dispersibility in blood stream.[23] When intravenously applied, the nanoparticles are usually recognized as foreign body and are

cleared through macrophages of the mononuclear phagocytosis system.[24] Therefore, the modification of surface became necessary for MR imaging through improving the stability and escaping the macrophage. Several approaches have been developed for converting hydrophobic surface to hydrophilic one, including ligand exchange,[9, 25] bipolar molecule stabilization[7] and polymer encapsulation.[22,26] These modifications endow SPIONs with reducing the possible protein adsorption, and consequently may result in improved stability in vivo. In addition, though SPIONs could be degraded into iron ions once upon uptaked into lysosome filled with acid and enzymes, numbers of studies have demonstrated that the toxicity or cytotoxicity of SPIONs is very limited in human even if at doses of 100 μg/mL or higher.[27]

In addition, our studies have shown that integration of the non-biodegradable block copolymer PEG-PEI and SPIO may result in a highly sensitive MRI probe capable of delivering siRNA. Consequently, siRNA accumulation in the tumor sites and evaluation of therapy effect could be readily achieved in nude mice bearing subcutaneously implanted tumors including human HCC xenografts.[10, 28] Yet, the vector biodegradability remains a challenging issue unsolved.

Very recently, we successfully synthesized a ternary copolymer mPEG-b-PLL-g-(ss-lPEI) (PLI) by grafting low molecular weight linear polyethylenimine (lPEI) onto the diblock copolymer of poly(L-lysine) (PLL) and poly(ethylene glycol) (PEG) through a disulfide linkage.[18] Grafting of low molecular lPEI significantly decreases the toxicity of PEG-b-PEI.[19] The grafted lPEI was confirmed to be cleavable from the copolymer in reducing environments such as inside cancer cells. Moreover, the PLL polypeptide backbone is assumed to maintain biodegradable because its amino side groups were partially and randomly grafted with lPEI only. High siRNA delivery efficiency has been achieved based on this ternary copolymer.

In the present study, we aimed to further develop a biodegradable vector which combines the siRNA delivery function with noninvasive MRI detection. To this end, SPIO was complexed with the above mentioned ternary copolymer PLI. To test its siRNA delivery efficiency, the MRI-visible vector was employed to deliver siRNA against survivin (sur-siRNA) into human HepG2 cancer cells. Admittedly, the MRI-visibility potentially facilitates the optimization of vector structure and treatment regimen design towards high delivery efficiency and good therapeutic outcome.

2. Experimental section

2.1. Materials

The biodegradable and reducible copolymer PEG-b-PLLys-g-(ss-lPEI), denoted as PLI, was synthesized as we recently reported.[18] The copolymer was then complexed with SPIO via ligand exchange. The HCC cell line HepG2 was obtained from the Institute of Biochemistry and Cell Biology, the Chinese Academy of Sciences (Shanghai, China). Dulbecco's Modified Eagle Medium (DMEM), Penicillin-Streptomycin, Fetal bovine serum (FBS) and Dulbecco's phosphate buffered saline (PBS) were purchased from Gibco BRL (Carlsbad, CA, USA). 3-(4,5-Dimethyl-thiazol-2-yl)-2,5-diphenyltetrazolium bromide (MTT) was obtained from Sigma-Aldrich (St. Louis, MO, USA). The fluorescent staining agent 4', 6-diamidion-2-phenylindole (DAPI) was purchased from Roche (Roche, Germany). AlexaFluor 555 was purchased from Molecular Probes (Invitrogen, USA). The siRNA duplexes purchased from Genpharm (Shanghai, China) have the sequences as follows: survivin siRNA: 5'-CACCGCAUCUCUACAUUCAdTdT-3' (sense), 5'-UGAAUGUAGAGAUGCGGUGdTdT-3' (antisense); scrambled siRNA (SCR): 5'- CACGCCAUCUCUAUCACUAdTdT-3' (sense), 5'- UAGUGAUAGAGAUGGCGUGdTdT-3' (antisense). Terminal deoxynucleotidyltransferase (TdT)-mediated dUTP nick end-labeling (TUNEL) kit, rabbit anti-human Survivin antibody and HRP-conjugated goat anti-rabbit antibody were purchased from Cell Signaling Technology (Danvers, CST, USA).

2.2 Preparation of SPIO labeled PEG-b-PLLys-g-(ss-lPEI) (PLI-SPION)

2.2.1 Synthesis of PEG-b-PLL-g-(ss-lPEI) (PLI)

PEG_{45}-b-$PLLys_{42}$-g-(ss-$lPEI_{15}$)$_{10}$ was synthesized as follows: 1.0 g of mPEG-b-PLL (0.135 mmol) was dissolved in 20 mL DMSO at room temperature for 30 min. Subsequently, another 20 mL DMSO solution containing 0.19 g NHS (1.65 mmol) and 1.08 g lPEI-COOH (1.35 mmol) was placed in a flask equipped with a magnetic stirring bar. The flask was cooled down to 18 °C in water bath, and then sealed off under argon after adding DCC (0.34 g, 1.68 mmol). The NHS-activated PEI solution was stirred at 18 °C for 1 h and then slowly added into the solution of mPEG-b-PLL. The reaction mixture was stirred at 18 °C for 1 h and then stirred at room temperature for 24 h. The precipitated DCU was removed by ultrafiltration. The filtrate was dialyzed against DI water for 4 days to remove organic solvents and then freeze-dried to obtain the mPEG-b-PLL-g-(ss-lPEI) polymer. The prepolymers lPEI-NH_2, lPEI-COOH and mPEG-b-PLL were synthesized as reported (see Supplementary information).[18]

2.2.2 Synthesis of water soluble Fe_3O_4 nanoparticles (WSPIO)

The hydrophilic Fe_3O_4 nanoparticles were synthesized as reported. [6-7] Briefly, the mixture of iron(III) acetylacetonate (2 mmol), 1,2-hexadecanediol (10 mmol), oleic acid (6 mmol), oleylamine (6 mmol), and benzyl ether (20 mL) in a reaction flask was magnetically stirred while it was heated to 200 ℃, reacted for 2 h and finally refluxed for another 1 h at 300 ℃ under argon. The black mixture was cooled down to room temperature, precipitated into ethanol and then centrifuged (12 000 rpm, 10 min) to remove the solvent. The black-brown hydrophobic Fe_3O_4 nanoparticles measuring 6 nm were re-dispersed into hexane. The hexane solution (0.2 mL) containing Fe_3O_4 nanoparticles (20 mg) was added to a solution of tetramethylammonium 11-aminoundecanoate in dichloromethane (10 mg mL^{-1}). The obtained mixture was shaken for 20 min, during which the hydrophilic particles precipitated out of the solution. The supernatant was discarded, and the precipitate was washed three times with dichloromethane to remove excess surfactants before drying under argon. The product was dispersed in deionized water prior to use.

2.2.3 SPION encapsulation with PLI (mPEG-b-PLLys-g-(ss-lPEI))

SPION encapsulated with PLI (PLI-SPION) was prepared referring to a ligand exchange method.[8-9] In brief, water soluble SPION (20 mg) was added into the aqueous solution of PLI (20 mg/mL). The above mixture was then magnetically stirred overnight at room temperature, and filtered through a 450 nm membrane to remove large aggregates. The products were washed

five times with deionized water and concentrated by centrifugal ultrafiltration. Finally, the solution was filtered through a 220 nm filter membrane and stored at 4 ºC.

2.3 Preparation of polyplex and determination particle size and zeta potential of siRNA complexation

The appropriate amount of PLI polymer solution was added into a vial containing predetermined (e.g., 1 μg) amount of siRNA. The mixture was vortexed for 30 s and then allowed to incubate with oscillation for 30 min at room temperature. A series of polyplexes were prepared at different N/P ratios ranging from 0 to 40, which were calculated as the ratio of nitrogen atoms in the PLI polymer to that of the phosphate groups in siRNA. The hydrodynamic sizes and zeta potentials of polyplexes of PLI-SPION and siRNA were determined via dynamic light scattering (DLS). Measurements were performed at 25 °C by using 90° Plus/BI-MAS equipment (Brookhaven Instruments Corporation, USA). For the zeta potential measurements, a standard electrophoresis mini-cell from Brookhaven was used. The data for particle size and zeta potential were collected on an auto-correlator with a detection angle of scattered light at 90° and 15°, respectively. For each sample, the data from ten measurements were averaged.

2.4 Confocal laser scanning microscopy (CLSM)

The intracellular distribution of the FITC-labeled siRNA and AlexaFluor 555 labeled polymer were detected using CLSM. About 1×10^4 HepG2 cells were seeded in the Petri dishes with a 40 mm glass bottom and incubated overnight in 1 mL of DMEM supplemented with 10% FBS. Polyplexes formed at the N/P ratio of 10 were added to the dishes. After 6 h, the cells were washed three times with PBS, and their nuclei were stained with DAIP (Sigma, USA) for 15 min at 37 °C. The fluorescence of cells was observed under a FluoView FV1000 microscope (OLYMPUS, Japan). FITC, AlexaFluor 555 and DAPI were excited at 494, 553 and 345 nm, and the green, red and blue fluorescence emissions of these molecules were observed at 518, 568 and 455 nm, respectively.

2.5 *In vitro* study

The HepG2 cells were seeded in six-well plates at a density of 1×10^5 cells per well and incubated overnight in 1 mL of DMEM containing 10% FBS. The transfection experiments were carried out as follows：40 μL solution of polyplex formed at N/P 10 was added to each well at varied siRNA concentrations of 25, 50, 100 and 200 nM to incubate the cells for 4 h. The medium was replaced with the same volume of fresh DMEM medium containing 10% FBS, and then the cells were further incubated for 48 h. The apoptotic cells were estimated with TUNEL assay. The expression of target gene was analyzed with real-time PCR, western blotting and immunocytochemical method.

2.5.1 *In vitro* MRI scan

HepG2 cells were seeded on 6-well plates at a density of 1×10^5 cells per well and incubated in the DMEM medium for 4 h in the presence of PLI-SPION/SCR at Fe concentrations of 0.2, 0.4, 0.6, and 0.8 μM separately. After being washed three times with PBS, the cells were trypsinized, resuspended in a 4% gelatin solution and monitored with a 1.5 T MR scanner (GE Healthcare UK Limited, Buckinghamshire, UK). A wrist coil with an inner diameter of 3 inches was used for the cell imaging. The T_2-weighted images were acquired using the following parameters: repetition time/echo time 5000/100 ms; FOV, 150 mm; matrix, 256 × 256; slice thickness, 1 mm. The signal intensities of the PBS control and PLI-SPION/SCR treated cells were determined using a circular 30 mm2 region of interest. The relative signal intensity of treated cells was normalized by comparison with that of control cells.

2.5.2 Quantitative real-time PCR assay for survivin mRNA level

Total RNA was isolated from the cells using the RNeasy Micro Kit (Qiagen Inc., USA), and mRNA was reverse transcribed into cDNA using PrimeScript® RT reagent Kit (Takara Biotechnology, Japan). The mRNA expression of survivin was quantified using a StepOne Plus real-time PCR System (ABI, USA). The cDNA sample (2 μL) was added into 18 μL of the PCR reaction mixture containing primers, FastStartTM Universal Probe master reagent (Roche Applied Science, Mannheim, Germany). The mRNA level of β-actin gene was used as an internal normalization standard. The PCR thermal cycling condition was as follows: 50 °C/2 min, 95 °C/10 min, and 40 cycles of 95 °C /15 s and 57 °C /60 s.

2.5.3 Western blot

Total protein was extracted using an M-PER TM total mammalian protein extraction reagent (thermo fisher, Darmstadt, Waltham, USA), and the total protein content was determined using a bicinchoninic acid protein assay kit (Invitrogen, Carlsbad, CA). About 10 μg of protein was separated on 12% SDS-PAGE in the tank (Bio-rad, Hercules, CA) and then transferred to a nitrocellulose membrane. The membranes were then incubated with rabbit anti-human survivin monoclonal antibody (1:500 dilution in PBS/Tween; Cell Signaling Technology, Danvers, USA). β-actin protein was used as an internal standard to normalize protein expression, and the protein-containing membranes were simultaneously incubated with β-actin monoclonal antibodies (1:2000 dilution in PBS/Tween; Santa Cruz Biotechnology Inc., Santa Cruz, CA). Protein-antibody complexes were detected via chemoluminescence (ECL Plus, Amersham Biosciences, USA).

2.5.4 TUNEL assay

The cells were plated at a density of 1×10^5 cells per well in 6-well plates and were incubated overnight at 37 °C. The polyplexes were added into the wells to induce apoptosis of the tumor cells. After 48 h cell incubation, TUNEL assay was performed using a FragELTM DNA fragment detection kit (colorimetric-TdT enzyme method) following the manufacturer's protocol (EMD chemicals Inc., Darmstadt, Germany). In brief, the cells were incubated with medium containing proteinase K (20 μg/mL) for 20 min at room temperature and then washed three times with TBS. The 3% H_2O_2 aqueous solution was used to inactivate the endogenous peroxidase at room temperature, and then the cells were washed with PBS. After treated with terminal deoxynucleotidyltransferase (TdT Enzyme) at 37 °C for 90 min, the exposed 3'-OH ends of the DNA fragment in the apoptotic cells can be labeled with biotin-labeled deoxynucleotides. After being washed three times with PBS, the cells were incubated with a streptavidin-horseradish peroxidase conjugate for 30 min at room temperature. Diaminobenzidine was added to react with the labeled deoxynucleotides to generate an insoluble brown DAB signal in the apoptotic cells. A shaded blue-green to greenish tan indicated the presence of non-apoptotic cells.

2.6 *In vivo* studies

All animal experiments were approved by the Institutional Animal Care and Use Committee of the Sun Yat-sen University. Female nude BALB/c mice were ordered from Vital River Laboratories (Beijing, china). HepG2 cells were implanted subcutaneously in 4 to 6-week old nude mice. Cells (1×10^6) in 100 μL of PBS were subcutaneously injected in the right back, and tumor growth was recorded via caliper measurements. Tumor volume was calculated using the following equation: volume = $0.5 \times L \times W^2$, where W and L are the width and length of the tumor, respectively.

The mice bearing tumor were randomly divided into three groups as follows (n = 20): (1) PLI-SPION complexing survivin siRNA (sur-siRNA) group, (2) PLI-SPION complexing scrambled siRNA (SCR) group, (3) PBS group. When the tumor volume reached approximately 50 mm^3 to 70 mm^3, administration of different formulations was conducted. Survival rate was analyzed using a log-rank test based on the Kaplan-Meier survival analysis by using MedCalc statistical software.

The tumors were excised and fixed for 24 h in 10% PBS buffered paraformaldehyde. After deparaffinization, tumor tissue sections (5 μm) were stained with hematoxylin/eosin (H&E) method. At least ten tumor sections from each animal were used for H&E staining. Immunohistochemistry study was then performed. The tumor sections were deparaffinized with xylene and alcohol, washed three times with PBS and incubated in 10 mM citrate buffer (pH 7.4) at 90 °C for 15 min. The sections were treated with 0.3% hydrogen peroxide in methanol at 4 °C for 30 min to inactivate the endogenous peroxidases. After being blocked with 10% normal horse serum, 2% bovine serum albumin, and 0.5% Triton X-100 for 1 h at room temperature, the tissues were incubated in the presence of rabbit polyclonal primary antibodies for survivin (1:500 dilution in PBS/Tween; Cell Signaling Technology, Danvers, USA) for 1 h at 37 °C, washed with PBS, and then further incubated for 1 h with horseradish-conjugated donkey anti-rabbit IgG secondary antibodies (DAKO Corporation, Carpinteria, CA). Finally, the immuno-reactivity on the tissue sections was detected by using the peroxidase substrate diaminobenzidine. Moreover, apoptosis in tumor sections was detected via TUNEL assay. For the molecular biology assays, tumor tissues were homogenized after being frozen in liquid nitrogen.

2.7 Statistical analysis

Data were statistically analyzed using one-factor analysis of variance (SPSS software, version 13.0, SPSS Inc.). The results were expressed as mean ± SE, and $P < 0.05$ was considered to indicate statistical significance. All statistical tests were two-sided.

3. Results and discussion

In the past few decades, some progresses have been achieved in liver cancer therapy. However, the lack of noninvasive approaches to monitor the therapeutic process and outcome has become a big problem when seeking for optimized regimens for ideal treatment effect. In this context, the emerging theranostic concept was considered to bring about great opportunity for the improvement of cancer therapy. In our recent study, the theranostical agent based on PEG-PEI showed good performance in gene delivery and MR imaging.[9] However, this non-biodegradable vector using high molecular weight PEI may lead to accumulative toxcicity when it was used in vivo. Therefore, in the present study we further developed a new theranostical agent based on a potentially biodegradable copolymer, the low molecular weight linear PEI grafted PEG-PLL,[18] in the hope of improving the biosafety and meanwhile maintaining the good theranostical function of vector (Fig. 1).

3.1 Synthesis and characterization of SPIO-labeled polyplex

The water soluble SPIO nanoparticles (WSPIO) with negative surface charge were prepared by mixing hydrophobic SPIONs with tetramethylammonium 11-aminoundecanoate, and showed an average diameter of 5 nm with uniform size distribution (Fig.2A). The PLI copolymer was complexed with WSPIO using a ligand exchange method.[9] The Fe loading content is 36.90%, as determined using the atomic absorption method. As shown in Fig.S1, the magnetization loops of the water soluble SPIONs (WSPIONs) and PLI-SPION@SCR were tested at both 10 K and room temperature. Both the WSPIONs and PLI-SPION@SCR appeared ferromagnetic at 10 K. The coercivities were 189 Oe and 197 Oe for WSPIONs and PLI-SPION@SCR, respectively. At room temperature, both nanoparticles were superparamagnetic, with zero coercivity. The saturation magnetization values were 79 Fe emu g^{-1} and 71 Fe emu g^{-1} for WSPIONs and PLI-SPION@SCR, respectively. The above results indicate that polymer coating had no obvious effect on the magnetic properties of SPIONs, which is essential for PLI-SPION@SCR to be used as a sensitive MRI probe. Finally, siRNA was complexed with PLI-SPION via electrostatic interaction to obtain the MRI-visible polyplex (PLI-SPION/siRNA) (Fig. 1). TEM observation showed that polyplex of 50 to 70 nm encapsulating several SPIONs in each particle has been obtained (Fig. 2B).

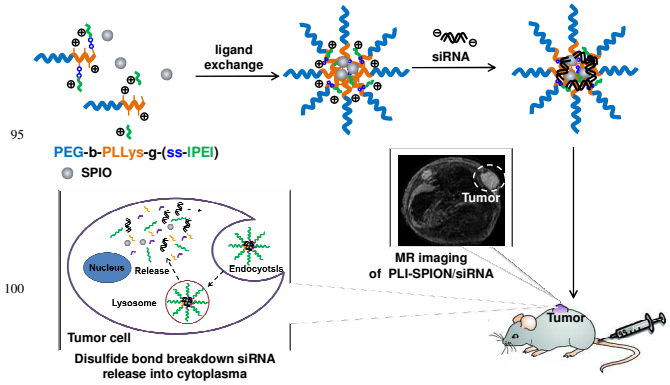

Fig. 1. Illustration of polyplex preparation, internalization into cancer cells and tumor MR imaging.

The capacity of PLI-SPION to complex siRNA at varied N/P ratios was analyzed with agarose gel electrophoresis. The motion of siRNA in electric filed was retarded due to the electrostatic neutralization. Complexation with SPION decreased somewhat the siRNA-complexing ability of PLI. As shown in Fig.S2, siRNA has been completely complexed by PLI at N/P 4. By contrast, siRNA was completely complexed by PLI-SPION above N/P 6, probably due to the loss of positive charge of PLI when some amino groups interacted with the negatively charged SPION. The siRNA complexation of PLI-SPION was also

studied by measuring the size and zeta potential of polyplex with dynamic light scattering (DLS) (Fig.2C). The particle size decreased from 110 to 85 nm following the increase of N/P ratio, and maintained around 60 nm above N/P 10. On the contrary, the zeta potential of polyplex increased along with the increase of N/P ratio, leveling off above N/P 17 to show a zeta potential around +22 mV. Since a low positive charge and small particle size of polyplex may facilitate siRNA delivery into cells[29], the polyplex formed at N/P 10 was selected for biological studies. The serum stability of PLI-SPION/siRNA was shown in Fig.2D. No obvious change in nanoparticle size was detected upon incubation with PBS or PBS plus 10% FBS. The small size and low positive charge might have contributed to the serum stability of PLI-SPION/siRNA. In addition, the complexation of PLI and SPION might have stabilized the nanoparticles in serum as well. [9, 30]

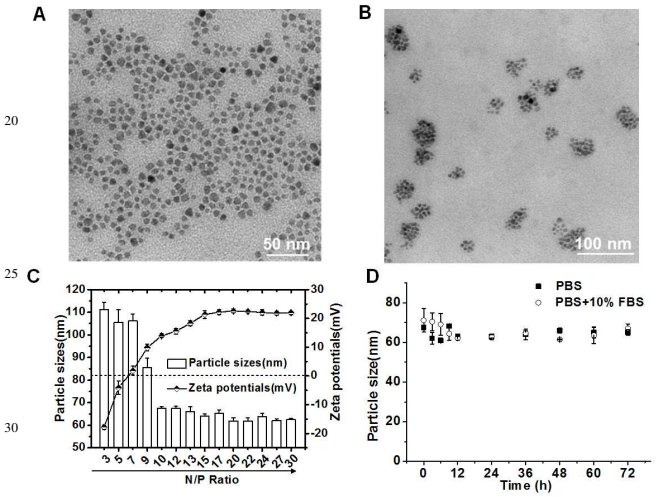

Fig. 2. Size and morphology of WSPIO (A) and PLI-SPION (B) analyzed transmission electron microscopy (TEM). Determination of Particle sizes and zeta potentials of the PLI-SPION/SCR polyplexes formed at various N/P ratios by dynamic light scattering (DLS) (C). Serum stability of PLI-SPION/SCR (N/P 10) measured by D LS at 37 °C (D).

3.2 Cytotoxixity study

The cytotoxicities of non-biodegradable PEG-PEI, biodegradable PLI and PLI-SPION were evaluated by MTT assay. As shown in Fig.S3, PLI and PLI/SPION both exhibited much lower cytotoxicity than PEG-PLL, suggesting that grafting low molecular weight lPEI to PEG-PLL greatly improved the biocompatibility of vector and meanwhile encapsulation of SPIO did not generate additional cytotoxicity. The cytotoxicities of polyplexes were evaluated at various N/P ratios as well. As shown in Fig.S3B, the cell viability gradually decreased along with increasing the N/P ratio for both the SPIO-free and SPIO-labeled polylexes. Moreover, the PLI-SPION/SCR of N/P 10 showed very low cytotoxicity. About 95% of the cells remained viable, which further rationalized our selection of the polyplex formed at N/P 10 for biological studies.

3.3 In vitro cell uptake

To show the cell uptake of siRNA mediated by PLI-SPION, the polymer and siRNA were labeled with AlexaFluor 555 and FITC, respectively. As shown in Fig.3A, after incubation with the magnetic polyplex of N/P 10, the HepG2 cells showed intracellular distribution of the green fluorescence (siRNA) identical to that of the red fluorescence (vector), leading to yellow fluorescence in the merged image. This result strongly demonstrates that siRNA was delivered into the cells by PLI-SPION.

The transfection efficiencies of polyplexes of various N/P ratios were determined by flow cytometry. As shown in Fig.3B and C, the polyplex obtained at N/P 10 showed the highest transfection efficiency (67%), presumably due to the small particle size, moderately positive charge and low cytotoxicity as confirmed by the DLS and MTT analyses. In contrast, the large particle size and negative surface of polyplexes formed at lower N/P ratios hindered the cell uptake, and the polyplexes formed at higher N/P ratios were more cytotoxic. Apparently, these factors are not favorable for the cell transfection of polyplexes.

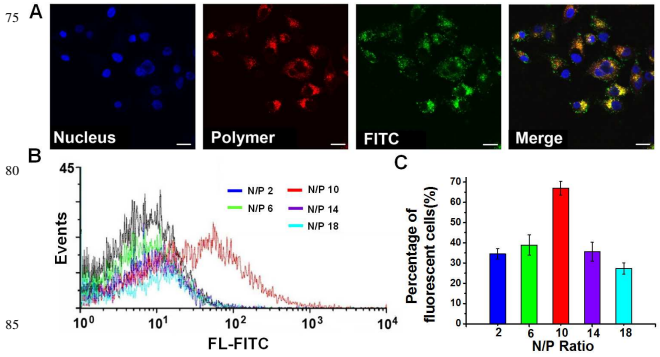

Fig. 3. (A) Laser confocal microscopic images of HepG2 cells after incubation with PLI-SPION/SCR (N/P 10). The blue, red and green fluorescences indicate the Hochest 3324 labeled nuclei, Alexa Fluor 555 labeled polymer and FITC labeled SCR, respectively. (B & C) Effect of N/P ratio on HepG2 cell uptake of polyplex, as evaluated by flow cytometry analysis of FITC-positive cells. Cell incubation time: 4 h. The scale bars represent 5 μm.

3.4 Ability of MR imaging in vitro and in vivo

The MRI-visible polyplex of N/P 10 exhibited higher T2 relaxivity (r^2 = 88.03 Fe mM^{-1} s^{-1}) than WSPIO (r^2 = 50.51 Fe mM^{-1} s^{-1}), indicating high MRI T_2-weighted imaging sensitivity (Fig. 4A and B). Prussian blue staining of cells after transfection with PLI-SPION/SCR showed that SPIO were delivered into the HepG2 cells, and the distribution of SPIO particles was similar to that of siRNA (Fig.4C). That is, SPION and siRNA were both located in cytoplasm in the studied cell incubation time. The above results show that the SPIO-labeled PLI may be a promising MRI-visible non-viral vector, which drove us to further study the siRNA delivery aiming to inhibit the expression of antiapoptotic survivin gene in a MRI-trackable manner.

The potential of tumor imaging with PLI-SPION/siRNA as a MRI probe was investigated in nude mice bearing human HepG2 xenograft. Polyplex solution was injected through tail vein at a dose of 10 mg Fe/kg body weight, and then the tumor targeted delivery was assessed on a 1.5 *T* MRI scanner. For MR imaging, the differences of spin relaxation kinetics of water hydrogen nuclei along the longitudinal and transverse planes are collected on MRI scanner to rebuild the tissue image in the applied magnetic field. It is well-known that the MRI T_2 contrast agent such as SPION can decrease the signal intensity by shortening

hydrogen transverse (spin-spin) relaxation time (T_2), and thus amplify the imaging differences by darkening the interfered area. Therefore, SPION-based MRI probe can be used to show the tumor tissue. Owing to its high sensitivity to detect the signal changes caused by iron particles,[9, 22, 26] the T_2-weighted gradient-recalled echo (GRE) sequences were used to monitor the accumulation of SPIO in the tumor site at various post-injection times. As shown in Fig.5A and B, tumor showed a clear darkening phenomenon and decrease of T_2-weighted signal intensity from 0.5 h to 18 h after injection of PLI-SPION/SCR (N/P=10). The signal intensity decreased gradually from 0.5 h to 3 h and until the lowest value (a decrease by 50.16±5.03%) at 3 h after polyplex injection, indicating the buildup of SPION in tumor. Then, the MR signal intensity of tumor gradually recovered due to the clearance of polyplex. At the time point of 18 h, it recovered by 90.97±3.94% (Fig.5B). Tumor accumulation of SPION-encapsulated PLI was also clearly shown in MRI T_2 mapping of the mice (Fig.5C).

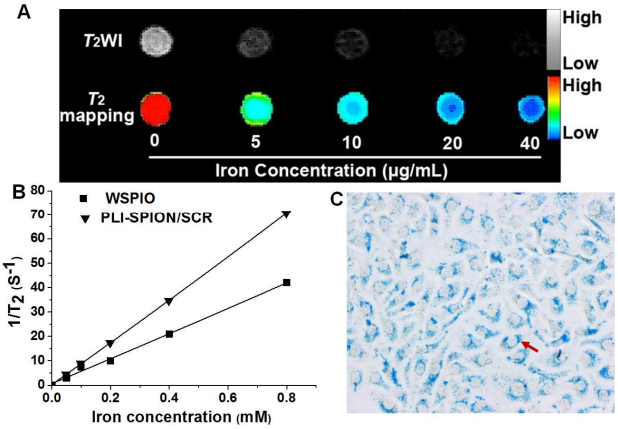

Fig. 4. (A) T_2-weighted (T_2WI) and T_2-mapping images of the HepG2 cells incubated with PLI-SPION/SCR at various Fe concentrations (μg/mL). (B) Magnetic resonance T_2 relaxation rate of WSPIO and PLI-SPION/SCR. (C) Prussian blue staining for SPIONs distribution inside cells incubated with PLI-SPION/SCR. The red arrow marked the SPIONs. Cell incubation time: 4 h. Polyplex prepared at N/P 10.

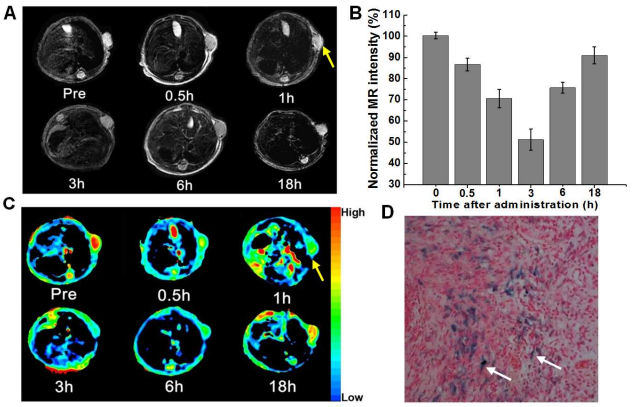

Fig. 5. (A) T_2-weighted images of mice bearing HepG2 tumor before and after tail vein injection of PLI-SPION/SCR (Dose: 10 mg Fe/kg body weight). (B) The signal intensity of T_2-weighted imaging normalized by comparison with that of the muscle tissue. (C) MRI T_2 mapping of mice receiving PLI-SPION/SCR. (D) Prussian blue staining of tumor sections excised from mice receiving PLI-SPION/SCR. The yellow and white arrows marked tumor and locations of SPIO, respectively. Polyplex prepared at N/P 10.

The histological study was performed with prussian blue staining on tumor tissue obtained 3 h after polyplex injection, which strongly support the in vivo MRI results. Tumor sections excised from mice receiving PLI-SPION/SCR demonstrated blue staining in tumor parenchyma (Fig.5D). These results imply that PLI-SPION is not only a potent siRNA carrier but also a potential MRI probe for tumor detection.

3.5 Suppression of survivin gene expression

Admittedly, survivin plays an important role in regulating cell apoptosis by functioning as an inhibitor of cell death. Up-regulation of survivin gene has been reported to account for poor prognosis in HCC, and down-regulation of survivin may lead to apoptosis of HCC tumor cell.[13-14, 31] Therefore, in the present study, sur-siRNA was complexed with PLI-SPION and then delivered into HepG2 cells in order to silence the survivin gene. PBS and scrambled siRNA (SCR) were used as negative controls for cell incubation.

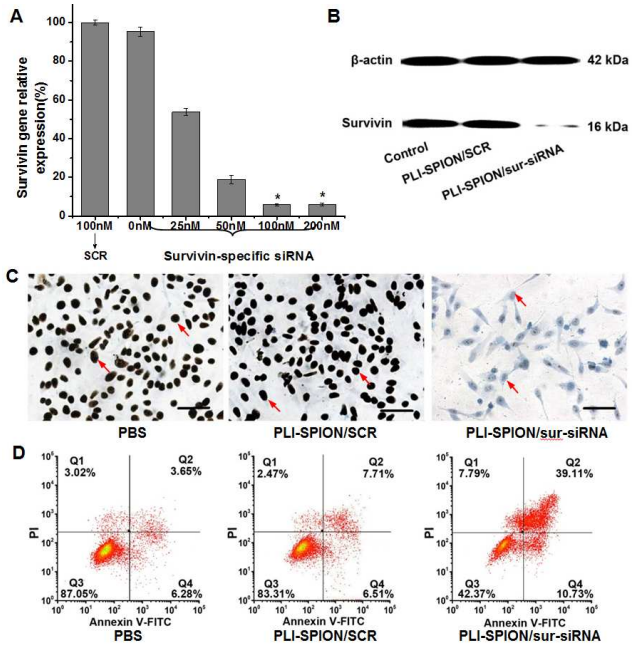

Fig. 6. (A) Efficiency of siRNA in suppressing survivin gene expression in HepG2 cells, as quantitatively determined by real-time PCR. Both sur-siRNA and SCR were delivered with PLI-SPION at N/P 10; *P<0.05 vs 50 nM sur-siRNA. (B) Survivin protein bands determined by western blotting. (C) Immunocytochemical analysis of survivin protein in HepG2 cells after incubation with 100 nM sur-siRNA. Incubation time: 48 h. The red arrow marked the nuclei. The scale bars represent 25 μm. (D) Cell apoptosis determined by flow cytometry after 48 h cell incubation with PBS, PLI-SPION/SCR and PLI-SPION/sur-siRNA, respectively. Q1: necrotic cells; Q2: late stage apoptotic cells; Q3: normal viable cells; Q4: early stage apoptotic cells.

The down-regulation of survivin gene expression was quantitatively evaluated by real-time PCR at mRNA level after HepG2 cell were treated with various amounts of sur-siRNA. The gene-silencing efficiency increased significantly with raising the siRNA concentration, reaching a saturation (about 95% down-

regulation) above 100 nM siRNA. By contrast, SCR showed no survivin gene suppression even at the high concentration of 100 nM (Fig.6A). Therefore, siRNA dose was fixed to 100 nM in the following experimental studies. Then, the suppression of survivin gene expression in HepG2 cell was tested at protein level. The SCR-incubated cells and normally cultured cells showed almost the same survivin protein level. However, as illustrated in Fig.6B and Fig.S4, the survivin protein level of cells was significantly lowered upon incubation with PLI-SPION/sur-siRNA. The Immunocytochemistry staining of survivin protein in HepG2 cells also showed that, in comparison with PLI-SPION/SCR, PLI-SPION/sur-siRNA could significantly reduce survivin protein in nuclei. (Fig.6C). The apoptotic and necrotic HepG2 cells induced by PBS, SCR and sur-siRNA were quantified by flow cytometry. The percentages of early apoptotic (Q4), late apoptotic (Q2), necrotic (Q1) and live cells (Q3) were shown in Fig.6D. Cells of the PBS and negative SCR control groups showed very low apoptotic activity. In comparison, cells of the sur-siRNA group exhibited much more remarkable apoptosis ($P < 0.05$). That is, the ratio of apoptotic cells was about 49.84±4.36% for the sur-siRNA group, which was significantly higher than that for the PBS group (9.93±0.47%) and negative siRNA (scrRNA) group (14.22±3.74%). The above data clearly evidenced that the suppression of survivin expression with PLI-SPION/sur-siRNA resulted in apoptosis of HepG2 cells.

Since the magnetic polyplex (PLI-SPION/sur-siRNA) demonstrated good biocompatibility, high siRNA transfection efficiency, and high MR sensitivity in vitro, further study was conducted to explore whether an effective siRNA therapy may also be achieved in vivo.

3.6 *In vivo* therapeutic effect of PLI-SPION/sur-siRNA

The therapeutic effect of PLI-SPION/sur-siRNA was investigated in nude mice bearing subcutaneous HepG2 xenografts. The tumor volumes and body weights were measured every 2 days up to 30 days. Starting from day 14, the tumor volume of mice receiving PLI-SPION/sur-siRNA group was much smaller than that of mice receiving PBS or PLI-SPION/SCR. In addition, there was no significant difference between the PBS group and PLI-SPION/SCR group (Fig.7A). For example, on the 26th day, the tumor volumes were 841.9±67.9 mm^3, 2261.5±122.8 mm^3 and 2107.3±199.6 mm^3 for the sur-siRNA group, SCR group and PBS group, respectively. The accumulative survival rates of mice obtaining different treatments were in line with the results of tumor growth inhibition. The death of mice in the sur-siRNA group, SCR group and PBS group began from day 28, 22 and 20, respectively. Moreover, 75% mice receiving PLI-SPION/sur-siRNA survived longer than 30 days, whereas 75% mice died within 30 days when receiving PLI-SPION/SCR (Fig.7B). Obviously, sur-siRNA delivered by the MRI-visible vector exerted desirable therapeutic effect in vivo.

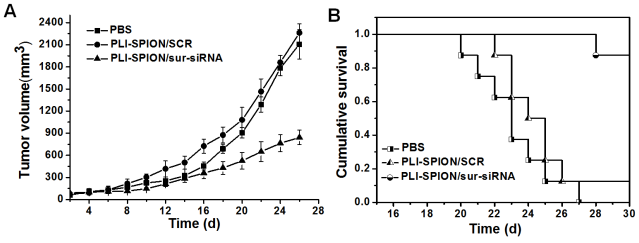

Fig. 7. Tumor growth inhibition (A), and cumulative survival rate (B) of mice bearing HepG2 liver carcinoma after various treatments (n=20).

H&E staining, immunochemical and TUNEL assays were further performed on the tumor tissue sections. As shown in Fig.8, typical tumor pathological features, such as hypercellular and nuclear polymorphism, were observed in the PBS and SCR control groups. Notably, mice receiving sur-siRNA showed the highest level of tumor necrosis. Since PLI and SPION have been demonstrated to have no obvious toxic effect *in vivo*,[8, 18] tumor necrosis in mice receiving PLI-SPION/sur-siRNA was mostly attributable to the therapeutic effect of sur-siRNA. Compared to mice receiving SCR, the mice receiving sur-siRNA showed much lower level of survivin protein (Fig.8). Finally, TUNEL assay also showed the highest level of apoptosis in tumor tissues of animals receiving PLI-SPION/sur-siRNA. These results demonstrated that tumor growth inhibition in the PLI-SPION/sur-siRNA group was due to the down-regulated survivin expression caused by sur-siRNA, as confirmed in the in vitro study as well.

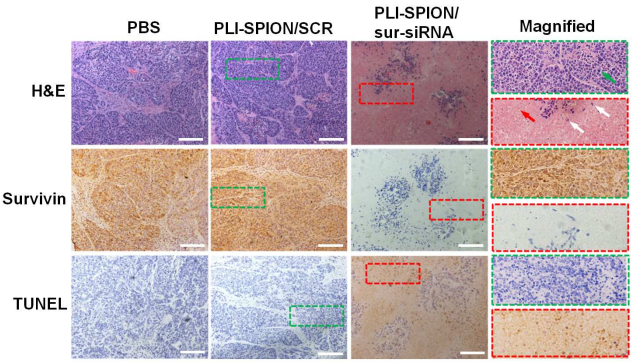

Fig. 8. Ex vivo histological analysis of tumor tissue sections. The H&E staining, immunohistochemical and TUNEL analyses of tumor tissue sections from mice treated with PBS or polyplex formed at N/P 10. The green rectangular area in the section of PLI-SPION/SCR and red rectangular area in the section of PLI-SPION/sur-siRNA were magnified. The green, white and red arrows mark normal tumor cells, apoptotic cells with chromatin or nuclei fragmentation and dead cells, respectively. The brown stains indicate survivin in the immunohistochemical assay and apoptotic cells in the TUNEL assay, respectively. The scale bars represent 50 μm.

Conclusions

A potentially biodegradable nanocarrier, PLI-SPION, was prepared to simultaneously deliver survivin-specific siRNA and MRI contrast agent SPIO. PLI-SPION effectively complexed sur-siRNA via electrostatic interaction and transported siRNA into HepG2 cells. Systematic biological studies demonstrated that, upon suppressing survivin expression with sur-siRNA, cancer cell apoptosis was induced to result in tumor growth inhibition. Moreover, the MRI visibility of vector enabled facile monitoring of the siRNA delivery. This study verifies the potential of PLI-SPION as a promising theranostical system combining effective siRNA delivery and high MRI sensitivity for imaging-assisted tumor therapy.

Acknowledgements

We gratefully acknowledge the financial support from the National Basic Research Program of China (2015CB755500), the National Natural Science Foundation of China (51225305, 21174166, 51373203 and 81271562), the Guangdong Innovative and Entrepreneurial Research Team Program (Grant No. 2013S086), the Natural Science Foundation of the Guangdong Province (S2012020011070), Special Project on the Integration of Industry, Education and Research of Guangdong Province (2013B090500094) and the Science and Technology Project of GuangZhou (2012J4100084).

Notes and references

[a] *Department of Radiology, The Third Affiliated Hospital of Sun Yat-sen University, Guangzhou 510630, China. Fax: +86-20-84112245; Tel: +86-20-84112172; E-mail: wangjin21cn@163.com*
[b] *PCFM Lab of Ministry of Education, School of Chemistry and Chemical Engineering, Sun Yat-sen University, Guangzhou 510275, China. Fax: +86-20-84112245; Tel: +86-20-84112172; E-mail: chengdu@mail.sysu.edu.cn; E-mail: shuaixt@mail.sysu.edu.cn*
[c] *Center of Biomedical Engineering, Zhongshan School of Medicine, Sun Yat-Sen University, Guangzhou 510080, China. Fax: +86-20-84112245; Tel: +86-20-84110365; E-mail: shuaixt@mail.sysu.edu.cn*

† Electronic Supplementary Information (ESI) available: See DOI: 10.1039/b000000x/

* Corresponding author.

Reference

1 D. Yoo, J. Lee, T. Shin, J. Cheon, Acc. Chem. Res., 2011, **44**, 863.
2 S.M. Janib, A.S. Moses, J.A. MacKay, Adv. Drug Delivery. Rev., 2010, **62**, 1052.
3 G. Lin, W. Zhu, L. Yang, J. Wu, B. Lin, Y. Xu, Z. Cheng, C. Xia, Q. Gong, B. Song, H. Ai, Biomaterials, 2014, **35**, 9495.
4 H. Zhang, L. Wang, Q. Xiang; Q. Zhong, L. Chen, C. Xu, X. Xiang, B. Xu, F. Meng, Y. Wan, D. Deng, Biomaterials, 2014, **35**, 356.
5 N. Schleich, C. Po, D. Jacobs, B. Ucakar , B. Gallez,, F. Danhier, V. Préat , J. Control. Release, 2014, **194**, 82.
6 Q. Sun, D. Cheng, X. Yu, Z. Zhang, J. Dai, H. Li, B. Liang, X. Shuai, J. Mater. Chem., 2011, **21**, 15316.
7 S. Sun, H. Zeng, D. B. Robinson, S. Raoux, P. M. Rice, S. X. Wang, G. Li, J. Am. Chem. Soc., 2004, **126**, 273.
8 G. Chen, , W. Chen, , Z. Wu, R. Yuan, H. Li, J. Gao, X. Shuai, Biomaterials, 2009, **30**, 1962.
9 Y. Guo, W. Chen, W. Wang, J. Shen, R. Guo, F. Gong, S. Lin, D. Cheng, G. Cheng, X. Shuai, ACS nano, 2012, **6**, 10646.
10 C. Wu, F.M. Gong, P.F. Pang, M. Shen, K.S. Zhu, D. Cheng, Z. Liu, H. Shan, PloS one, 2013, **8**, e66416.
11 B. Li, Q. Tang, D. Cheng, C. Qin , F.Y. Xie, Q. Wei, J. Xu, Y. Liu, B.J. Zheng, M.C. Woodle, N.S. Zhong, P.Y. Lu, Nat. Med., 2005, **11**, 944.
12 A. de Fougerolles, H.P. Vornlocher, J. Maraganore, J. Lieberman, Nat. Rev. Drug Disco., 2007, **6**, 443.
13 S. Shin, B.J. Sung, Y.S. Cho, H.J. Kim, N.C. Ha, J.I. Hwang, C.W. Chung, Y.K. Jung, B.H. Oh, Biochemistry, 2001, **40**, 1117.
14 F. Li, G. Ambrosini, E.Y. Chu, J. Plescia, S. Tognin, P.C. Marchisio, D.C. Altieri. Nature, 1998, **396,** 580.
15 S. Peroukides, V. Bravou, A. Alexopoulos, J. Varakis, H. Kalofonos, H. Papadaki, Histol.Histopathol., 2010, **25**, 299.
16 G. Salzano, R. Riehle, G. Navarro, F. Perche, G. De Rosa, V.P. Torchilin. Cancer lett., 2014, **343**, 224.
17 K.A. Whitehead, R. Langer, D.G. Anderson, Nat. Rev. Drug Discov., 2009, **8**, 129.
18 J. Li, D. Cheng, T. Yin, W. Chen, Y. Lin, J. Chen, R. Li, X. Shuai, Nanoscale. 2014, **6**, 1732.
19 J. Dai, S. Zou, Y. Pei, D. Cheng, H. Ai, X. Shuai. Biomaterials, 2011, **32**, 1694.
20 J. Dai, S. Lin, D. Cheng, S. Zou, X. Shuai, Ang. Chem.Int. Ed., 2011, **50**, 9404.
21 J.W.M. Bulte, D.L. Kraitchman, NMR Biomed., 2004, **17**, 484.
22 D. Cheng, G. Hong, W. Wang, R. Yuan, H. Ai, J. Shen, B. Liang, X. Shuai, J. Mater. Chem., 2011, **21**, 4796.
23 Wong, X. W. Teng, X. Z. Lin and H. Yang, Nano Lett., 2003, **3**, 1555.
24 L.H. Reddy, J.L. Arias, J. Nicolas, P. Couvreur, Chem. Rev., 2012, **112**, 5818.
25 U. I. Tromsdorf, N. C. Bigall, M. G. Kaul, O. T. Bruns, M. S. Nikolic, B. Mollwitz, R. A. Sperling, R. Reimer, H. Hohenberg, W. J. Parak, S. Fo1rster, U. Beisiegel, G. Adam, H. Weller, Nano Lett., 2007, **7**, 2422.
26 H. Ai, C. Flask, B. Weinberg, X. Shuai, M.D. Pagel, D. Farrell, J. Duerk, J. Gao, Adv. Mater., 2005, **17**, 1949.
27 N. Singh, G. J.S. Jenkins, R. Asadi, S.H. Doak, Nano Rev., 2010, **1**, 5358.
28 M. Shen, F. Gong, P. Pang, K. Zhu, X. Meng, C. Wu, J. Wang, H. Shan, X. Shuai. Int. J. Nanomed., 2012, **7,** 3319.
29 Z. Medarova, W. Pham, C. Farrar, V. Petkova, A. Moore, Nat. med., 2007, **13**, 372.
30 H. Wei, R. Zhuo, X. Zhang, Prog. Polym. Sci., 2013, **38**, 503.
31 Y.P. Yen, K.S. Tsai, Y.W. Chen, C.F. Huang, R.S. Yang, S.H. Liu, Arch. Toxicol., 2012, **86**, 923.

